Viscoelasticity mapping by identification of local shear wave dynamics

Viscoelasticity Mapping by Identification of Local Shear Wave Dynamics

Ruud J. G. van Sloun, Rogier R. Wildeboer, Hessel Wijkstra, and Massimo Mischi

***Abstract*— Estimation of soft tissue elasticity is of interest in several clinical applications. For instance, tumors and fibrotic lesions are notoriously stiff compared with benign tissue. A fully quantitative measure of lesion stiffness can be obtained by shear wave (SW) elastography. This method uses an acoustic radiation force to produce laterally propagating SWs that can be tracked to obtain the velocity, which in turn is related to Young's modulus. However, not only elasticity, but also viscosity plays an important role in the propagation process of SWs. In fact, viscosity itself is a parameter of diagnostic value for the detection and characterization of malignant lesions. In this paper, we describe a new method that enables imaging viscosity from SW elastography by local model-based system identification. By testing the method on simulated data sets and performing *in vitro* experiments, we show that the ability of the proposed technique to generate parametric maps of the viscoelastic material properties from SW measurements, opening up new possibilities for noninvasive tissue characterization.**

***Index Terms*— Elastography, ultrasonic imaging, signal analysis.**

I. Introduction

IMAGING technologies for assessment of the elastic properties of soft tissue provide clinicians with an important asset for several diagnostic applications. Pathologies, such as tissue fibrosis and cancer influence tissue elasticity. Accurate detection and staging of these pathologies is fundamental for providing adequate treatment and disease management. For this purpose, manual palpation is used extensively in clinical routine. Among the elastographic possibilities, ultrasound enables remote palpation using acoustic radiation force: shear wave (SW) elasticity imaging. By applying a push-pulse using high-intensity focused ultrasound, tissue is locally displaced in the axial direction, causing the formation of a laterally propagating SW. If one considers the medium to be purely elastic, its local shear modulus can be estimated by determining the local SW speed.

In practice, the assumption of pure elasticity, however, does not hold for many tissue types; tissue in which not only the stiffness, but also the shear viscosity plays an important role. Moreover, there is increasing evidence that viscosity itself could be a discriminant parameter for the detection of malignancy. Hoyt *et al.* [1] assessed the elastic properties of prostate cancer tissue for their relevance as biomarkers. Their results revealed that the viscosity of cancerous prostate tissue is greater than that derived from normal tissue. Therefore, in this paper, we aim at providing a joint estimate of tissue elasticity and viscosity based on SW elastography.

Initially, inversion of the Helmholz equation was used to reconstruct SW speed from time–displacement data [2], [3]. However, calculating the required second-order derivatives in space and time makes such an estimator very susceptible to the noisy signal conditions one can expect *in vivo*. More recently developed methods assess SW speed by calculating the wave arrival time across a set of axial displacement curves. In [4] and [5], SW speed was obtained by assessing the lateral time-to-peak and exploiting linear regression to determine the rate-of-change across the set. Later, a more robust version of this approach was developed [6], in which a random sample consensus (RANSAC) algorithm was employed to reliably perform such a regression in the presence of strong outliers. Rouze *et al.* [7] showed that the SW time-of-flight can also be estimated using a Radon sum transformation, yielding a comparable robustness with respect to the RANSAC algorithm. An alternative approach determined the local SW speed by cross correlating the displacement waveform at a specific position with that obtained at a reference location [8]. All of the above-mentioned methods operate under the explicit assumption of negligible viscous dispersion across the evaluated region, translated in negligible wave shape deformation.

To assess the SW dispersion that originates from viscosity, Nenadic *et al.* [9] devised a method that relates the 2-D Fourier transform (2-D-FT) of time–displacement data to the frequency-dependent SW phase velocity. By calculating the wavenumber (spatial frequency) that maximizes the spectrum at a given temporal frequency, the phase velocity at each frequency can be obtained, which in turn can be parameterized using typical viscoelastic material models, such as the Voigt model [10]. However, obtaining sufficient spatial frequency resolution to perform an accurate and reliable phase velocity estimate requires the use of a relatively large amount of space points. This seriously hampers its applicability to high-resolution mapping of viscosity. Rouze *et al.* [11] proposed the use of a lookup table that relates the viscosity-driven difference in estimated SW group speed between axial particle velocity and displacement to the viscoelastic material parameters. Another elastographic imaging method aims at assessing the viscoelastic material parameters by estimating

Manuscript received July 13, 2017; accepted August 18, 2017. Date of publication August 23, 2017; date of current version October 24, 2017. This work was supported in part by the Dutch Cancer Society under Grant UVA2013-5941 and in part by the European Research Council Starting Grant under Grant 280209. *(Corresponding author: Ruud J. G. van Sloun.)*

R. J. G. van Sloun, R. R. Wildeboer, and M. Mischi are with the Laboratory of Biomedical Diagnostics, Eindhoven University of Technology, 5600 MB Eindhoven, The Netherlands (e-mail: r.j.g.v.sloun@tue.nl).

H. Wijkstra is with the Laboratory of Biomedical Diagnostics, Eindhoven University of Technology, 5600 MB Eindhoven, The Netherlands, and also with the Academic Medical Center, University of Amsterdam, 1000 GG Amsterdam, The Netherlands

Digital Object Identifier 10.1109/TUFFC.2017.2743231

the mechanical relaxation time for a radiation-force-induced stress [12]. In [13], single-tracking-location viscoelasticity estimation was proposed, in which viscosity was quantified through model-based quantification of wave dispersion of two laterally spaced push pulses at a single tracking location.

In this paper, we consider the viscoelastic material as a dynamic linear system, of which the impulse response can be locally identified by input–output (point-to-point) analysis of SW time–displacement curves. To this end, a local model-based estimator of the impulse response is derived from the Navier–Stokes equation, which is then fit to the data in a least-squares fashion.

The SW data acquisition protocol and preprocessing steps are given in Sections II-A and II-B, respectively. The details of the adopted signal model and an analytical description of the impulse response in viscoelastic materials are then given in Section II. This impulse response is identified from the acquired data, to provide an estimation of the viscoelastic model parameters, as reported in Section II-D. The method is validated using simulated SW measurements (Section III-A) and *in vitro* data sets (Section III-B1), and the results are presented in Section IV. Finally, in Section V, these results are discussed and conclusions derived.

II. Methods

A. Data Acquisition

The experiments were performed using a Verasonics Vantage 128 ultrasound research platform (Redmond, WA, USA) in combination with an L11-4 linear array transducer. SWs were generated with acoustic radiation force, where the mechanical impulse delivered to the tissue is given by the product of acoustical force density and duration. Hence, to facilitate sufficient medium displacement, a 1500-cycle push-pulse with a center frequency of 4.5 MHz was adopted (excitation-duration: 333 μs), and the excitation voltage was set to the maximum (overheating protected) value of 65 V. The resulting SW was tracked using an ultrafast imaging protocol operating at a frame rate of 10 kHz. A single-cycle pulse with a center frequency of 6.25 MHz was used. The in-phase & quadrature (IQ) data were reconstructed after dynamic receive beamforming of the radio frequency data, and stored for off-line processing. The final pixel dimensions in the axial and lateral directions were 0.086 mm and 0.208 mm, respectively. No additional averaging of repeated push-pulses was employed.

B. Preprocessing

To reveal the laterally propagating SW, we estimate its micrometer-scale axial displacements based on the well-known Loupass 2-D autocorrelator [14]. Initially developed for measuring blood flow velocity in Doppler systems, this approach estimates the mean axial velocity at each location by evaluating the 2-D autocorrelation function of the IQ samples within a specific axial range N_{ax} and frame/ensemble range N_{ens}. In our experiments, these values were set to $N_{\text{ax}} = 20$ samples (1.7 mm) and $N_{\text{ens}} = 5$ frames (500 μs), respectively. Finally, the axial velocity maps were spatially filtered using a 2-D Gaussian kernel with a standard deviation of 1.2 samples in both the axial and lateral directions.

C. Shear Wave Signal Model

For the purpose of estimating the SW propagation dynamics, we consider the displacement profiles measured at two laterally spaced pixels, and describe their relation as

$$u(x + \Delta x, t) = w(\Delta x, t) *_t u(x - \Delta x, t) \tag{1}$$

where $w(\Delta x, t)$ is the impulse response that characterizes the system describing the transition from $u(x - \Delta x, t)$ to $u(x + \Delta x, t)$. If one considers the SW propagation process as purely convective, the impulse response is a delayed delta function, and can be written as

$$w(\Delta x, t) = \delta\left(t - \frac{2\Delta x}{c_s}\right) \tag{2}$$

with c_s being the SW velocity. In this case, the model $w(\Delta x, t)$ can be identified by simply maximizing the cross correlation function between the two displacement profiles in order to find their time delay, and thereby the SW velocity. In viscoelastic media, SWs do not merely propagate in a convective manner; their shape also spreads over space. The Navier–Stokes equation provides us with a more general framework. Adopting the classical Voigt model to describe the viscoelastic properties of tissue [10], that is

$$\sigma(t) = (\mu_0 + \eta\partial_t)\epsilon(t) \tag{3}$$

with stress $\sigma(t)$, strain $\epsilon(t)$, stiffness $\mu_0 = \rho c_s^2$ (elastic spring), and viscosity η (dashpot), SW particle displacements can be written as follows [15]:

$$\rho\partial_t^2 u(\vec{r}, t) - \left(\rho c_s^2 + \eta_s\partial_t\right)\nabla^2 u(\vec{r}, t) = S(\vec{r}, t) \tag{4}$$

where ρ is the mass density and $S(\vec{r}, t)$ is the excitation source. The spatiotemporal impulse response of this system, termed the Green's function $g(\vec{r}, t)$, is then obtained by solving

$$\rho\partial_t^2 g(\vec{r}, t) - \left(\rho c_s^2 + \eta_s\partial_t\right)\nabla^2 g(\vec{r}, t) = \delta(\vec{r})\delta(t). \tag{5}$$

In one space dimension, x, (5) can be written in the 2-D Fourier domain as

$$-\rho\omega^2 G(k_x, \omega) + \left(\rho c_s^2 + j\omega\eta_s\right)k_x^2 G(k_x, \omega) = 1. \tag{6}$$

Equation (6) is derived specifically for a Voigt material. It can, however, be generalized to describe other material models in terms of a frequency-dependent shear modulus $\mu(\omega)$, such that we obtain

$$-\rho\omega^2 G(k_x, \omega) + \mu(\omega)k_x^2 G(k_x, \omega) = 1 \tag{7}$$

from which, we can derive the following Green's function solution:

$$G(k_x, \omega) = \frac{(1/\rho)}{[\mu(\omega)/\rho]k_x^2 - \omega^2}. \tag{8}$$

The inverse Fourier transform of (8) with respect to k_x is given by

$$G(x, \omega) = \frac{\sqrt{\pi/2}}{j\omega\rho\sqrt{\mu(\omega)/\rho}} \exp\left[-\frac{j\omega|x|}{\sqrt{\mu(\omega)/\rho}}\right]. \tag{9}$$

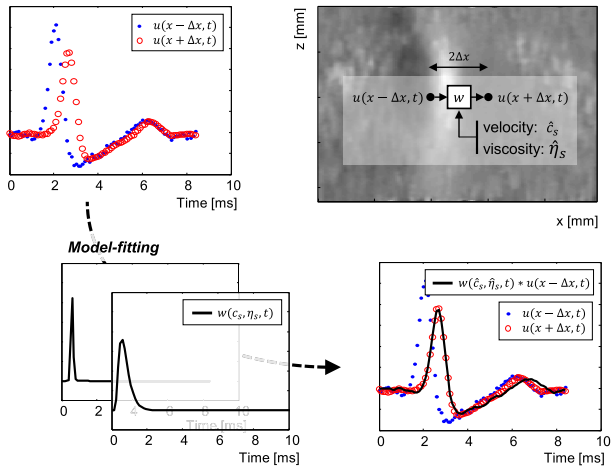

Fig. 1. Illustrative overview of the proposed method, showing how the point-to-point impulse response is estimated from the time–displacement curves sampled at two spatial locations $x - \Delta x$ and $x + \Delta x$.

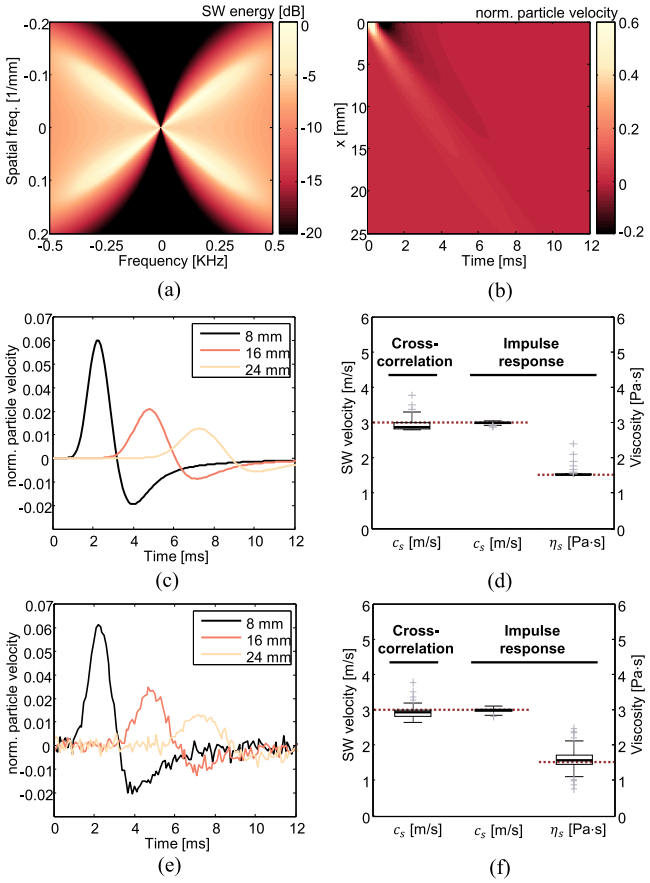

Fig. 2. Simulation of SW propagation in a viscoelastic material with $\mu_0 = 9$ kPa, $\rho = 1000$ kg/m^3, and $\eta_s = 1.5$ Pa·s based on [17]. (a) Generated 2-D Fourier domain SW data. (b) Resulting particle velocity in the space-time domain. (c) and (e) Several particle velocity signals at different lateral positions are shown as a function of time, with and without additive Gaussian white noise (standard deviation: 5% of peak amplitude at 10 mm), respectively. (d) and (f) Resulting SW velocity ($\hat{c}_s = (\mu_0/\rho)^{1/2}$) and viscosity estimates along the lateral position are summarized in box plots. Dotted line: true values. For comparison, the results for SW velocity estimation based on a cross correlation approach are also shown.

From (9), the impulse response $w(\Delta x, t)$ from one space point to another can be described in the frequency domain as

$$W(\Delta x, \omega) = \frac{G(|x| + 2\Delta x, \omega)}{G(|x|, \omega)} = \exp\left[-\frac{j\omega|2\Delta x|}{\sqrt{\mu(\omega)/\rho}}\right]. \quad (10)$$

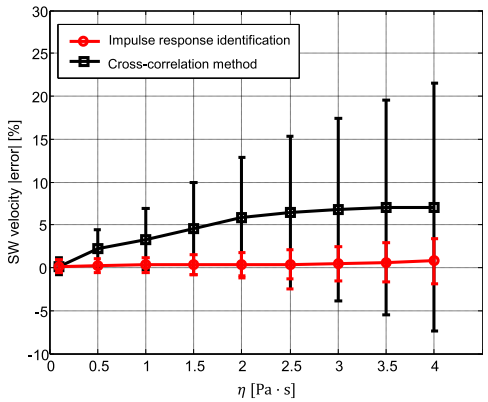

Fig. 3. SW velocity estimation errors in viscoelastic material simulations as a function of increasing viscosity. Bars: standard deviation of estimates across the lateral position. The proposed method is compared with a correlation-based time-of-flight method.

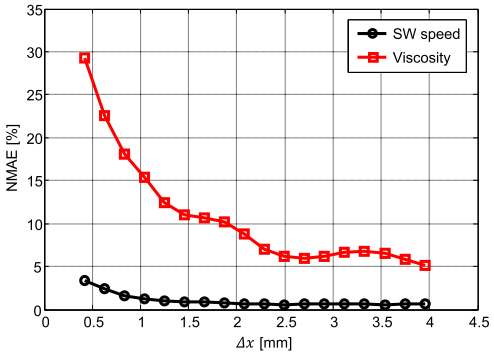

Fig. 4. Normalized mean absolute error of the SW velocity and viscosity estimates as a function of increasing lateral spacing Δx for a simulation with material parameters $\mu_0 = 9$ kPa and $\eta = 3$ Pa · s. Gaussian white noise (standard deviation: 5% of peak amplitude at 10 mm) was added to the particle velocity signals.

D. Shear Wave System Identification

To locally estimate the viscoelastic model parameters in the Voigt model [$\mu(\omega) = \rho c_s^2 + j\omega\eta_s$), from (1) to (10)], we formulate the following nonlinear least-squares problem:

$$\{\hat{c}_s, \hat{\eta}_s, \hat{\alpha}\}(x) = \min_{c_s,\eta_s,\alpha} \|\mathcal{F}^{-1}[W(\Delta x, \omega)V(x - \Delta x, \omega)] - v(x + \Delta x, t)\|_2^2 \quad (11)$$

where $V(x - \Delta x, \omega)$ is the temporal Fourier transform of $v(x - \Delta x, t)$, the axial particle velocity signal. This Fourier domain implementation of the convolution between $v(x - \Delta x, t)$ and $w(\Delta x, t)$ avoids aliasing that can occur when sampling the impulse response $w(\Delta x, t)$ in the time domain. Such a situation is likely to occur in a low-viscosity case, where $w(\Delta x, t)$ approximates a delta function. On the other hand, sampling in the Fourier domain on the bandwidth determined by the sample rate produces a filtered version of the impulse response, without aliasing in the time domain (corresponding to a shifted and sampled Sinc function for $\eta = 0$). In addition, the approach allows for a computationally efficient implementation via the fast Fourier transform. Equation (11) is numerically solved in an iterative fashion using a Nelder–Mead simplex algorithm [16]. We employed a course grid search across c_s and η_s (10 × 10) to select

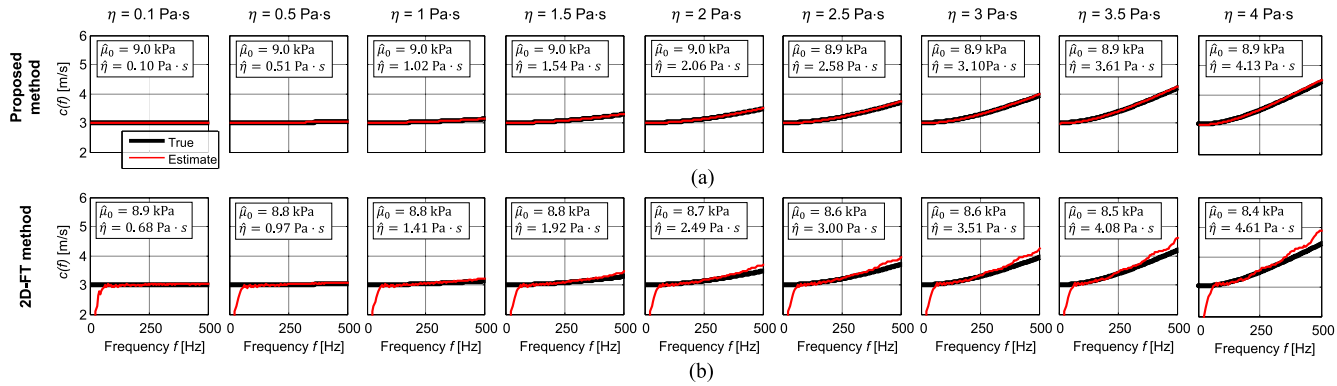

Fig. 5. Frequency-dependent phase velocity estimates compared with the true values for simulated particle velocity measurements in several Voigt materials (stiffness $\mu_0 = 9$ kPa, mass density $\rho = 1000$ kg/m^3, and varying viscosity $\eta = [0.1 - 4]$ Pa · s). The estimates based on (a) proposed method and (b) 2-D-FT method described by Nenadic *et al.* [9] are compared. For the latter, (13) is fit to the phase-velocity estimates in a frequency range of 70–500 Hz to obtain $\hat{\mu}_0$ and $\hat{\eta}$.

appropriate initial conditions. The median number of iterations to reach convergence was 93.

Fig. 1 gives an illustrative overview of the proposed method.

III. Validation Methodology

A. Simulation Study

The proposed method was first tested on simulated data sets by generating particle velocity measurements based on an analytic description of SW propagation in a viscoelastic medium following a Gaussian excitation as described in [17]. The cylindrically symmetric Gaussian excitation has the following form:

$$\vec{f}(r,t) = W(t)\exp(-|\vec{x}|^2/\sigma^2)\hat{z} \tag{12}$$

where $\hat{z}$ is the unit vector in the axial direction, $\sigma = 1$ mm gives the width, and $W(t)$ determines the time profile of the excitation: a rectangular window with a length of $T = 333$ μs. We adopted a Voigt material model with stiffness μ_0 and viscosity η, and generated nine realizations of SW particle velocity measurements in materials with different degrees of viscosity.

The data sets were then processed as described in Sections II-A–II-D in order to obtain estimates of SW velocity and viscosity as a function of the lateral position x. Δx was set to 1.25 mm. The results are compared with those obtained using a standard cross-correlation-based time-of-flight method for SW velocity estimation [8] with the same Δx, and a 2-D-FT approach for frequency-dependent SW phase velocity measurements [9]. The latter first calculates the 2-D-FT of the full spatiotemporal SW signal, after which the average phase velocity at a specific temporal frequency is retrieved by locating the spatial frequency at which the 2-D-FT is maximized: $c(f) = f/k_{\max}(f)$.

B. In Vitro Study

1) Phantom Design: In our experiments, commercially available tofu (Unicurd Food Company Pte Ltd., Singapore) served as a typical high-viscosity material. Because its elastographic and echographic properties are similar to those of some soft tissues, this poroelastic soy-based product has been used as a viscous tissue-mimicking phantom [18]. In [19], the effective Poisson's ratio ν of tofu was measured during 600 s of compression, displaying approximate incompressibility ($\nu \approx 0.5$) across the time frame of the measurements performed in this paper (10 s). To mimic low-viscosity tissues, water-based eight weight-% gelatin was prepared [20], [21]. It consisted of 20-g gelatin, 9.95-g graphite scattering powder, and 225-mL water. In total, we prepared three phantoms from these materials: two homogeneous phantoms (one tofu and one gelatin), and one tofu phantom with a cylindrical gelatin inclusion (diameter of 9 mm).

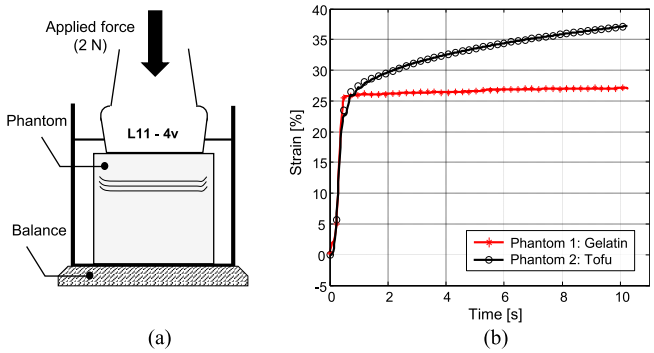

Fig. 6. (a) Ultrasound strain measurements upon application of a sudden stress. (b) Resulting creep curves for gelatin and tofu phantoms, showing a higher viscous creep for the latter.

2) SW Experiments: The SW experiments were performed as described in Section II-A. The data was then processed according to Sections II-A–II-D, with Δx set to 1.25 mm (i.e., six lateral samples).

3) Mechanical Characterization: A material's viscoelastic behavior can be directly estimated by assessing its creep curve, i.e., the time-dependent strain behavior upon the application of a constant load [18]. Considering a three-parameter material model consisting of a Voigt model with an elastic element in series, the instantaneous response to the compression is regarded as purely elastic, whereas the subsequent creep curve is attributed to the presence of viscosity [20]. The tofu and gelatin phantoms were cut into blocks of similar size (6 cm × 5 cm × 2 cm) and subjected to a precompression force of ≈ 0.35 N. Then, their axial strain was monitored after

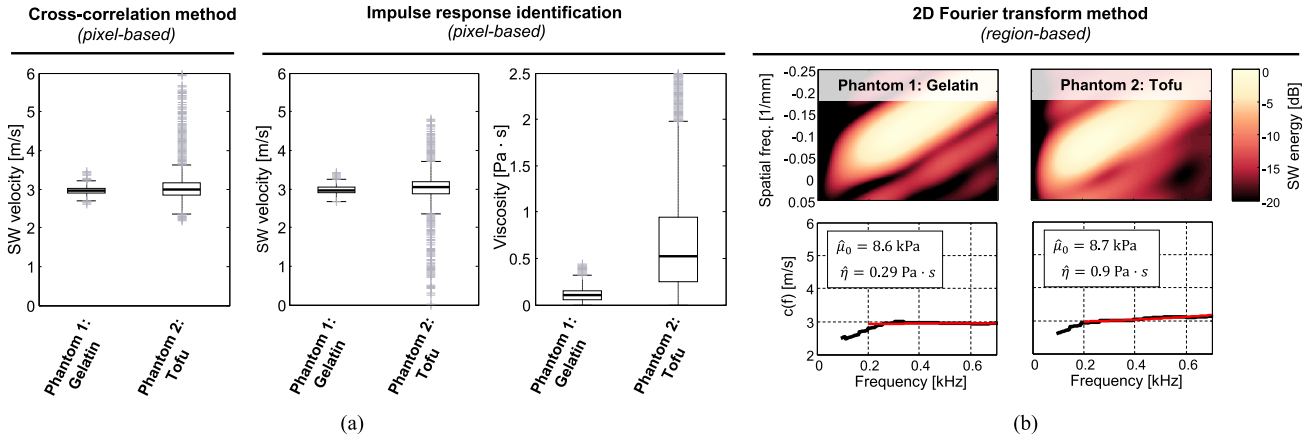

Fig. 7. (a) Box plots displaying the distributions of pixel-based estimates of SW velocity ($\hat{c}_s = (\mu_0/\rho)^{1/2}$) and viscosity in gelatin and tofu phantoms as obtained using the proposed method, compared with velocity estimates using a cross correlation-based time-of-flight method. Using cross correlation, the gelatin phantom yielded SW speeds with a median, mean, and standard deviation of 2.96, 2.79, and 0.70 m/s, respectively. For tofu, these values were 2.99, 2.87, and 0.79 m/s, respectively. Using the proposed method, the gelatin phantom yielded SW speeds with a median, mean, and standard deviation of 2.96, 2.80, and 0.71 m/s, respectively. For tofu, these values were 3.04, 2.87, and 0.80 m/s, respectively. The proposed method yielded viscosity values for gelatin with a median, mean and standard deviation of 0.10, 0.11, and 0.08 Pa · s, respectively. For tofu, these values were 0.53, 0.66, and 0.59 Pa · s, respectively. (b) Comparison with the 2-D-FT method [9] applied to the entire region.

the application of a sudden compressive load of about 200 g (2 N) across the footprint of the L11-4 linear array transducer.

For strain imaging during compression, ultrasound images were acquired at a frame rate of 50 Hz. Large frame-to-frame velocities (>1 sample/frame) were estimated by blockwise cross correlation of log-compressed B-mode frames (speckle-tracking), and fine subsample displacements were captured by estimating the axial velocity from the IQ data using the Loupass 2-D autocorrelator [14]. The ensemble and axial ranges were set to 5 frames and 30 samples, respectively. The axial frame-to-frame displacements were then tracked over time using a Kalman filter [22] to measure the relative strain at a set depth after velocity estimation.

IV. Results

A. Simulation Results

Fig. 2 shows an example of simulated data based on [17]. SW velocities c_s and material viscosities η_s are estimated along the lateral direction x based on the proposed method, and their distributions are summarized in box plots [Fig. 2(d)]. One can observe that the estimates are very close to the true values ($c_s = 3$ m/s and $\eta_s = 1.5$ kPa). Moreover, the SW velocity estimates seem to be slightly improved with respect to those obtained using the correlation-based time-of-flight approach [8]. The improved estimation of SW velocity in simulated data by considering viscosity in the estimation procedure can also be noted from Fig. 3. The estimates of SW velocity based on the proposed impulse response identification procedure yield lower errors and standard deviations compared with those obtained in a time-of-flight fashion, in particular for high viscosity.

The impact of altering the lateral spacing Δx (throughout this paper set to 1.25 mm) on the estimates is shown in Fig. 4. Overall, the estimation error decreases when increasing Δx, which comes at the price of a reduced spatial resolution.

Fig. 5 shows different degrees of SW phase-velocity dispersion resulting from various levels of viscosity. The frequency-dependent phase velocities were computed from the median estimates of η_s and c_s along the lateral direction x in the following manner [17]:

$$c(\omega) = \sqrt{\frac{2\left(\mu_0^2 + (\eta_s\omega)^2\right)}{\rho\left(\mu_0 + \sqrt{\mu_0^2 + (\eta_s\omega)^2}\right)}} \tag{13}$$

where the stiffness $\mu_0 = \rho c_s^2$. From the upper row of Fig. 5, one can notice that the estimates are very close to the true phase velocities for all simulations. The bottom row shows the results of the 2-D-FT method [9] applied to the full space-time data. Here, the estimated phase velocities deviate slightly from the true values, in particular for higher frequencies and viscosity.

B. In Vitro Results

The creep curves presented in Fig. 6 show how the gelatin and tofu phantoms display different time-strain behavior. When subjected to a sudden stress, gelatin compresses instantly and shows little to no creep, whereas the tofu phantom creeps significantly and clearly presents more viscous behavior.

Fig. 7 summarizes the obtained pixel-based SW velocity and viscosity distributions for both phantoms when applying the proposed method. The SW velocity estimates are compared with those measured using the cross correlation approach. Moreover, we compared the parameter distributions to the values obtained using the 2-D-FT method. In line with the mechanical characterization, the estimated viscosity is significantly higher in tofu than in gelatin, while the velocity (and, therefore, stiffness) is not significantly different. While these characteristics are confirmed by the 2-D-FT method, we notice a difference in the absolute viscosity values that is similar to the 2-D-FT bias found in the simulation study

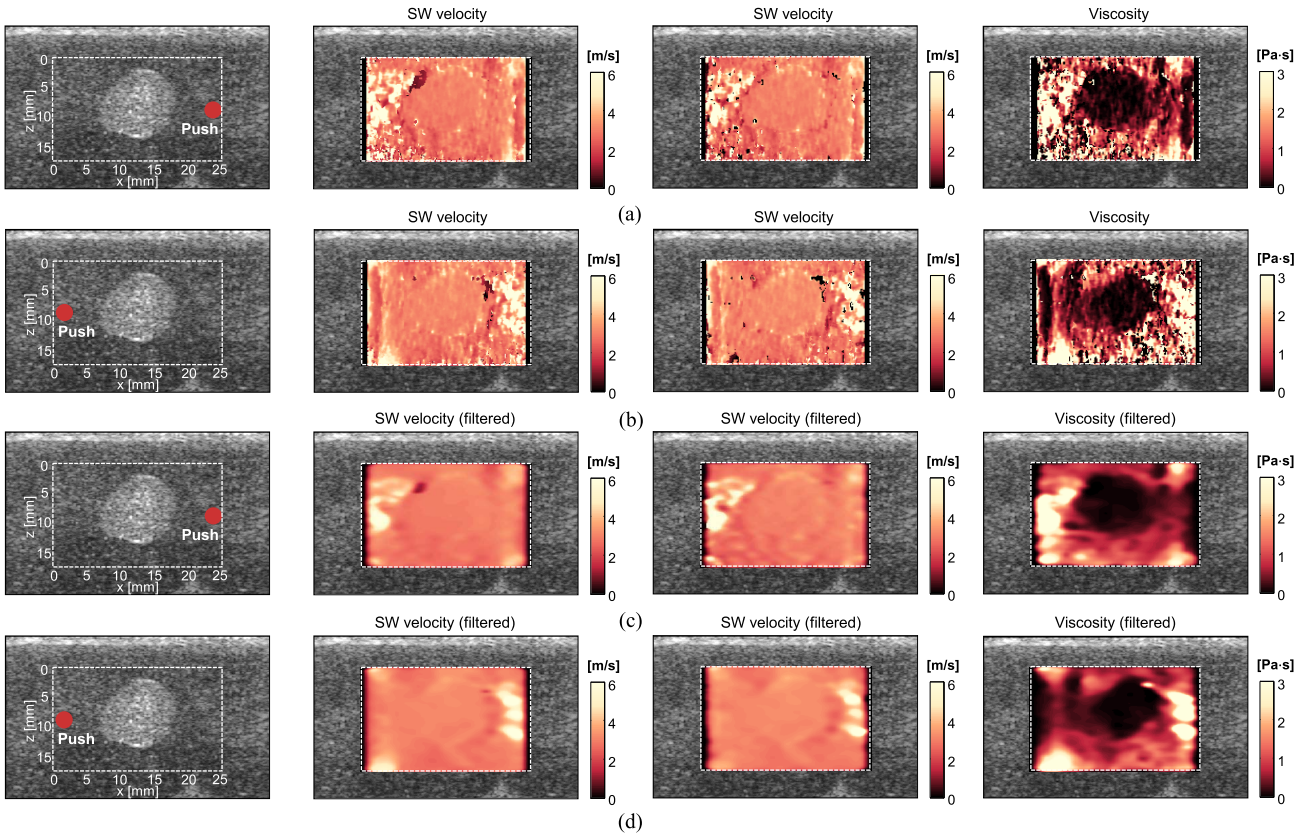

Fig. 8. Proposed SW viscoelasticity imaging on a tofu phantom containing a cylindrical inclusion of gelatin, as compared with a typical correlation-based time-of-flight elastographic approach. The results are given (a) and (b) without and (b) and (c) with spatial filtering. The maps obtained using an acoustic push focus positioned on the right lateral side (a) and (c) are compared with those obtained with a push on the left lateral side (b) and (d).

(see Fig. 5). The spread and range of estimated values is higher in the tofu phantom as compared with the gelatin phantom.

Finally, viscoelasticity imaging was performed on a tofu phantom containing a cylindrical inclusion of gelatin. The images were postprocessed using a 2-D median filter (kernel dimensions: 1 mm $\times$ 3.5 mm) followed by a 2-D Gaussian filter (standard deviation: 0.2 mm $\times$ 0.6 mm). From Fig. 8, one can appreciate that the less-viscous gelatin inclusion is indeed revealed by the viscosity maps, whereas the velocity images (portraying the purely elastic behavior) fail to expose it. Where the results obtained with a push-focus on either side of the imaging domain [Fig. 8(b) and (c)] qualitatively show great similarity in the central zone of the image, one can also observe that the estimates very close the push location and at the far end do not share the same degree of consistency.

V. Conclusion and Discussion

In this paper, a new approach to determine tissue viscoelasticity based on SW elastography is presented. By locally characterizing SW propagation using a system identification approach, the proposed method enables not only mapping of tissue elasticity, but also of viscosity. The developed technique extends beyond the typical time-of-flight based methods by estimating the kinetics between laterally sampled time–displacement curves instead of just their time delay.

The algorithm was first tested on simulated data sets, validating its technical correctness with respect to a well-defined ground truth. The assumption of negligible viscosity in a viscoelastic material leads to inadequate estimation of SW velocity based on time-of-flight. On the contrary, by jointly estimating SW velocity and material viscosity, the proposed method appropriately assesses both characteristics (Fig. 2).

The impact of viscosity on time-of-flight SW velocity estimates was further investigated on a range of simulations with viscous materials ($\eta = 0.1$ Pa $\cdot$ s to $\eta = 4$ Pa $\cdot$ s). As expected, the presence of viscosity impairs the time-of-flight estimates, yielding high standard deviations along the lateral position. Frequency-dependent attenuation causes lower frequencies (and their phase speeds) to become more dominant with increasing distance from the source, introducing a bias that depends on the lateral direction. The proposed method overcomes this issue by adequately modeling the effects of viscosity on SW propagation. As a result, the estimation errors and in particular their standard deviations are much smaller.

On the same range of viscous materials, the resulting phase velocities derived from the estimated material properties showed good agreement with true values (Fig. 5). Interestingly, we observed that the 2-D-FT method for phase velocity dispersion characterization displayed a bias, in particular for higher frequencies (toward 500 Hz) and viscosities. Such a bias was also noted by Rouze *et al.* [17]. In this regard, we would like to point out that the simulated range of η represents expected viscosities in tissue. Wang and Insana [23] investigated the

viscoelastic properties of fibroadenomas and carcinomas in rats by extracting and characterizing shear-velocity dispersion curves. Based on a Kelvin–Voigt model, they reported viscosity values that range from $\eta = 0.56$–3.54 Pa $\cdot$ s.

Based on the measured *in vitro* SW data, we found that the method yielded material-property estimates which confirmed the mechanical characterization of the material; tofu and gelatin have similar stiffness, yet very distinct viscosity. We point out that this comparison is qualitative: the material might be well described by a particular viscoelastic model and set of coefficients for one range of frequencies (creep experiment, up to 25 Hz), but then described by the same model with a different set of coefficients over a second, dissimilar, range of frequencies (SW experiment, up to 500 Hz). As noted in Section IV-B, the spread and range of estimated values was found higher in the tofu phantom as compared with the gelatin phantom. This may originate from substantial material heterogeneity in tofu, which is less evident in gelatin. Moreover, the degraded signal-to-noise level in tofu, which is caused by higher shear attenuation, may have impacted the estimation accuracy and thereby its variance. These practical aspects seem to overwelm the theoretically predicted decrease in variance for the SW velocity estimates by the proposed method, as observed in the simulation study.

By imaging a gelatin phantom with a cylindrical tofu inclusion, we showed that the method is able to generate a viscosity map that reveals the inclusion. The possibility of yielding such a viscosity map using ultrasonic SW elastography was already discussed in [15], where Bercoff *et al.* contemplated that adding viscosity maps in SW imaging could be of great interest for tumor characterization.

The artifacts in the viscosity maps that appear close to the acoustic push focus (Section IV-B) occur when estimating the model parameters from data in the SW near-field. We may speculate that these artifacts originate from:

1) Non plane wave propagation in the near-field, a condition for which our 1-D model does not hold.
2) The fact that the push-pulse is not a delta-Dirac in space, leading to the presence of an additional apparent "source" between the two lateral positions from which the impulse response is assessed. This violates the assumption that those two points only record a passing SW and all measured axial displacement originates from this propagating wave.

At the lateral far end, we also observe the presence of estimation artifacts. Here, wave aberration and low signal-to-noise ratio are likely degrading the estimates. The aforementioned artifacts can be mitigated by proper combination of estimates from several SW measurements obtained using different lateral push-foci [24]. Reliability can be assessed based on location (e.g., close to the push-focus) and signal quality. Such a multifocus strategy can also be pursued in the axial direction to cover a wide spatial range.

Compared with other methods that aim at assessing viscosity from SW measurements, we like to stress that the proposed method is able to generate estimates in a pixel-based point-to-point fashion. This approach enables the generation of SW maps with a lateral resolution that is primarily determined by the adopted spacing between these points (in this paper $2\Delta x$). Choosing a suitable Δx amounts to a tradeoff. Decreasing Δx leads to fine estimates, close to the lateral resolution of the U.S. acquisition. Yet, increasing Δx results in a more pronounced effect of the local material properties on the kinetics between the two points, accommodating a more robust estimation procedure in the presence of noise (see Fig. 4) and a higher sensitivity. The appropriate value depends on the application; for tumor localization, a resolution in the order of millimeters is required [25], whereas the characterization of diffuse hepatic steatosis may permit assessment on a larger scale [26].

The work presented in this paper shows parallels with [13], where Langdon *et al.* [13] describe a method that employs two laterally spaced push pulses to generate two time–displacement curves at a single-tracking-location. These curves are then used to estimate the material parameters of the material between the two push-foci. Where such an approach requires two push pulses for each lateral position at which one desires to estimate the viscoelastic parameters, our method only requires one push pulse to generate a full map of the viscoelastic parameters.

To confirm the practical utility of the prosed method, it should be tested extensively on real tissue. Such tests can initially be conducted *ex vivo*, but should eventually lead to *in vivo* experiments. In these conditions, the impact of noise, diffraction, and aberration, along with other disturbances, should be carefully investigated. The proposed method was applied to particle velocity signals which yield reduced low-frequency (motion) artifacts and a stronger signal morphology which is dominant on a more compact temporal support compared with displacement signals. Yet, particle velocity estimates are more susceptible to high frequency noise and hence require the use of more robust estimators. Although the method presented in this paper was applied to SW data obtained from a single push pulse, one can imagine that the high *in vivo* demands require strategies such as supersonic SW generation and SW compounding [3]. The former produces an intense source by generating SWs that interfere constructively along a Mach cone to boost the signal-to-noise ratio. The latter combines the results from multiple SWs to improve reliability of the estimates. Application of the proposed method in such a fashion is straightforward.

Besides improving the method reliability using a high-quality SW data set, we can also resort to more advanced system identification techniques based on maximum-likelihood estimators that take full advantage of the expected noise statistics to yield robust parameter estimates. Such approaches require a careful design of the noise model for SW displacement signals, considering the full acquisition chain from the push source to the (Loupass) displacement estimator and any subsequent preprocessing.

Although the results presented herein were obtained assuming a Voigt material model, the approach can be readily generalized to facilitate characterization in terms of other viscoelastic material models, such as the typically adopted Maxwell or three-parameter model. One would then merely need to select the appropriate frequency-dependent shear

modulus $\mu(\omega)$, and solve the minimization problem as described in (11) for the corresponding material parameters. It should be noted, however, that the optimization procedure for a three-parameter model with two stiffness constants is most-likely more challenging than for the two-parameter Maxwell and Voigt models.

If the proposed method's applicability is confirmed *in vivo*, it could in principle be readily implemented on any SW device without requiring hardware changes. This would open up new possibilities for the detection and characterization of pathologies based on their local viscoelasticity.

ACKNOWLEDGMENT

This research was conducted in the framework of the IMPULS2-Program at the Eindhoven University of Technology in collaboration with Philips.

REFERENCES

[1] K. Hoyt *et al.*, "Tissue elasticity properties as biomarkers for prostate cancer," *Cancer Biomarkers*, vol. 4, nos. 4–5, pp. 213–225, 2008.

[2] K. Nightingale, S. McAleavey, and G. Trahey, "Shear-wave generation using acoustic radiation force: *In vivo* and *ex vivo* results," *Ultrasound Med. Biol.*, vol. 29, no. 12, pp. 1715–1723, 2003.

[3] J. Bercoff, M. Tanter, and M. Fink, "Supersonic shear imaging: A new technique for soft tissue elasticity mapping," *IEEE Trans. Ultrason., Ferroelect., Freq., Control*, vol. 51, no. 4, pp. 396–409, Apr. 2004.

[4] M. L. Palmeri, M. H. Wang, J. J. Dahl, K. D. Frinkley, and K. R. Nightingale, "Quantifying hepatic shear modulus *in vivo* using acoustic radiation force," *Ultrasound Med. Biol.*, vol. 34, no. 4, pp. 546–558, 2008.

[5] M. H. Wang *et al.*, "*In vivo* quantification of liver stiffness in a rat model of hepatic fibrosis with acoustic radiation force," *Ultrasound Med. Biol.*, vol. 35, no. 10, pp. 1709–1721, 2009.

[6] M. H. Wang, M. L. Palmeri, V. M. Rotemberg, N. C. Rouze, and K. R. Nightingale, "Improving the robustness of time-of-flight based shear wave speed reconstruction methods using RANSAC in human liver *in vivo*," *Ultrasound Med. Biol.*, vol. 36, no. 5, pp. 802–813, 2010.

[7] N. C. Rouze, M. H. Wang, M. L. Palmeri, and K. R. Nightingale, "Robust estimation of time-of-flight shear wave speed using a radon sum transformation," *IEEE Trans. Ultrason., Ferroelect., Freq., Control*, vol. 57, no. 12, pp. 2662–2670, Dec. 2010.

[8] J. McLaughlin and D. Renzi, "Shear wave speed recovery in transient elastography and supersonic imaging using propagating fronts," *Inverse Problems*, vol. 22, no. 2, p. 681, 2006.

[9] I. Nenadic, M. W. Urban, B. Qiang, S. Chen, and J. Greenleaf, "Model-free quantification of shear wave velocity and attenuation in tissues and its *in vivo* application," *J. Acoust. Soc. Amer.*, vol. 134, no. 5, p. 4011, 2013.

[10] A. C. Eringen, *Mechanics of Continua*, vol. 1. Huntington, NY, USA: Krieger, 1980, p. 606.

[11] N. C. Rouze, Y. Deng, M. L. Palmeri, and K. R. Nightingale, "Robust characterization of viscoelastic materials from measurements of group shear wave speeds," in *Proc. IEEE Int. Ultrason. Symp. (IUS)*, Sep. 2016, pp. 1–4.

[12] M. R. Selzo and C. M. Gallippi, "Viscoelastic response (VisR) imaging for assessment of viscoelasticity in voigt materials," *IEEE Trans. Ultrason., Ferroelect., Freq., Control*, vol. 60, no. 12, pp. 2488–2500, Dec. 2013.

[13] J. H. Langdon, E. Elegbe, and S. A. McAleavey, "Single tracking location acoustic radiation force impulse viscoelasticity estimation (STL-VE): A method for measuring tissue viscoelastic parameters," *IEEE Trans. Ultrason., Ferroelect., Freq., Control*, vol. 62, no. 7, pp. 1225–1244, Jul. 2015.

[14] T. Loupas, J. T. Powers, and R. W. Gill, "An axial velocity estimator for ultrasound blood flow imaging, based on a full evaluation of the Doppler equation by means of a two-dimensional autocorrelation approach," *IEEE Trans. Ultrason., Ferroelect., Freq., Control*, vol. 42, no. 4, pp. 672–688, Jul. 1995.

[15] J. Bercoff, M. Tanter, M. Muller, and M. Fink, "The role of viscosity in the impulse diffraction field of elastic waves induced by the acoustic radiation force," *IEEE Trans. Ultrason., Ferroelect., Freq., Control*, vol. 51, no. 11, pp. 1523–1536, Nov. 2004.

[16] J. A. Nelder and R. Mead, "A simplex method for function minimization," *Comput. J.*, vol. 7, no. 4, pp. 308–313, 1965.

[17] N. C. Rouze, M. L. Palmeri, and K. R. Nightingale, "An analytic, Fourier domain description of shear wave propagation in a viscoelastic medium using asymmetric Gaussian sources," *J. Acoust. Soc. Amer.*, vol. 138, no. 2, pp. 1012–1022, 2015.

[18] R. Righetti, M. Righetti, J. Ophir, and T. A. Krouskop, "The feasibility of estimating and imaging the mechanical behavior of poroelastic materials using axial strain elastography," *Phys. Med. Biol.*, vol. 52, no. 11, pp. 3241–3259, 2007.

[19] A. Chaudhry, T. Krousko, P. Shajudeen, and R. Righetti, "Estimation of effective Poissons ratio in non-homogeneous porous media using two ultrasound transducers: A feasibility study," *Imag. Med.*, vol. 8, no. 4, pp. 105–111, 2016.

[20] M. Sridhar and M. F. Insana, "Ultrasonic measurements of breast viscoelasticity," *Med. Phys.*, vol. 34, no. 12, pp. 4757–4767, 2007.

[21] M. F. Insana, C. Pellot-Barakat, M. Sridhar, and K. K. Lindfors, "Viscoelastic imaging of breast tumor microenvironment with ultrasound," *J. Mammary Gland Biol. Neoplasia*, vol. 9, no. 4, pp. 393–404, 2004.

[22] R. E. Kalman, "A new approach to linear filtering and prediction problems," *J. Basic Eng.*, vol. 82, no. 1, pp. 35–45, 1960.

[23] Y. Wang and M. F. Insana, "Viscoelastic properties of rodent mammary tumors using ultrasonic shear-wave imaging," *Ultrason. Imag.*, vol. 35, no. 2, pp. 126–145, 2013.

[24] P. Song, A. Manduca, H. Zhao, M. W. Urban, J. F. Greenleaf, and S. Chen, "Fast shear compounding using robust 2-D shear wave speed calculation and multi-directional filtering," *Ultrasound Med. Biol.*, vol. 40, no. 6, pp. 1343–1355, 2014.

[25] T. A. Stamey, F. S. Freiha, J. E. McNeal, E. A. Redwine, A. S. Whittemore, and H.-P. Schmid, "Localized prostate cancer. Relationship of tumor volume to clinical significance for treatment of prostate cancer," *Cancer*, vol. 71, no. S3, pp. 933–938, 1993.

[26] T. Deffieux *et al.*, "Investigating liver stiffness and viscosity for fibrosis, steatosis and activity staging using shear wave elastography," *J. Hepatol.*, vol. 62, no. 2, pp. 317–324, 2015.

Authors' photographs and biographies not available at the time of publication.